Optical generation of vortices in trapped Bose-Einstein condensates

G. Andrelczyk,[1] M. Brewczyk,[1] Ł. Dobrek,[2] M. Gajda,[3] and M. Lewenstein[2]
[1]*Uniwersytet w Białymstoku, ul. Lipowa 41, 15-424 Białystok, Poland*
[2]*Institut für Theoretische Physik, Universität Hannover, 30167 Hannover, Germany*
[3]*Institute of Physics, Polish Academy of Sciences & College of Science, Al. Lotników 32, 02-668 Warsaw, Poland*
(Received 7 December 2000; published 10 September 2001)

We study theoretically a generation of vortices by phase imprinting in trapped Bose-Einstein condensates. Phase imprinting is achieved by passing a short off-resonance laser pulse through an appropriately designed absorption plate, and impinging it on a condensate. We answer the fundamental question how the circulation and the vortex are introduced into the system. We discuss the possibility of multiple vortex arrays creation. Using multiple absorption plates we show that genuine vortex arrays and vortex-antivortex configurations can be created in a controlled way. We discuss vortex dynamics and interactions in such configurations. Various methods of vortex detection based on interference combined with Bragg scattering technique are also analyzed.

DOI: 10.1103/PhysRevA.64.043601 PACS number(s): 03.75.Fi, 32.80.Pj, 42.50.Vk

I. INTRODUCTION

In recent years the studies of ultracold atomic gases have concentrated to a great extent on investigations of various aspects of superfluidity in Bose-Einstein condensates (BEC). One aspect concerns the existence of critical velocity for the dissipationless flow, which has been demonstrated by Raman *et al.* [1] and Onofrio *et al.* [2] (for theory see [3]). Perhaps more effort has been, however, devoted to the study of generation and dynamics of vortices in BEC [4–6]. These studies are related to the engineering of various collective excited states of BEC, such as ''scissors modes'' [7,8] and nontopological textures, such as dark solitons [9,10].

There are two different physical situations in which vortices can be investigated. In rotating traps vortices appear in a natural way as thermodynamic ground states with quantized angular momentum [11]. Stability and other properties of vortices in rotating traps has been thoroughly discussed in Refs. [12–14]. In the stationary trap the creation of vortices (or related dark solitons) requires the use of dynamical means and an independent stability analysis.

So far, two laboratories have been able to generate and study vortex dynamics. In the JILA experiment [6], atoms on the border of a single-component rubidium condensate ($F=1$, $m_F=-1$) are excited using a Raman transition to the state ($F=2$, $m_F=1$) in such a way that the resulting condensate wave function of the created condensate has an ''imprinted'' phase that corresponds to a vortex state. This method, proposed in Ref. [15], is very much related to the ''phase imprinting'' method discussed in the present paper. It corresponds to the creation of vortices in a nonrotating trap. In the experiment by Madison *et al.* [4] and Chevy *et al.* [5], a rubidium gas is evaporatively cooled while being ''stirred'' by a focused laser beam. ''Stirring'' can be kept on or turned off after the nucleation of vortices, corresponding to a rotating or nonrotating trap, respectively. In the ENS experiment not only have single vortices, but also vortex arrays have been observed. Perhaps the most challenging questions related to the above experiments concern dissipative dynamics of the ''birth and death'' of vortices, or vortex arrays, and in particular the theory of their nucleation, dynamical, and thermodynamic stability, and modes of decay [16].

Even though two successful experimental methods to create vortices have been demonstrated, it is, in our opinion, worth studying other possible vortex generation methods that might provide certain advantages over the two above-mentioned ones. There exist several theoretical proposals on how to generate vortices in nonrotating traps: stirring of the condensate using a blue detuned laser [17,18] or several laser beams [19], adiabatic passage [20], Raman transitions [21] in bicodensate systems, laser beam vortex guiding [22], or laser beam diffraction on a helical light grating [23]. In the present paper we concentrate on the method of ''phase imprinting'' using absorption plates that we have proposed in a recent Rapid Communication [24]. This method has been very successfully applied to generate solitons [9,10], and it offers specific kinds of control of the generation process, and thus the fascinating possibility of quantum state engineering. In the case of dark solitons it allows, for instance, not only for the creation of a single soliton, but also for the controlled engineering of multiple dark soliton textures [9].

The paper is organized as follows. In Sec. II A we explain what the ''phase imprinting'' method is and how it works. Note that this dynamical method allows us to introduce nonvanishing circulation into the originally noncirculating condensate. One of the fundamental questions is, therefore, how the circulation and the vortex are introduced into the system. This question is answered in this section. Section II B discusses the possibility of vortex array creation using the phase imprinting. We present here a ''phase diagram'' relating the array form to the parameters of the imprinting laser pulse. In Sec. III we extend our method to the use of multiple absorption plates that allow for genuine vortex array ''design.'' Section IV deals with the problem of vortex detection; we discuss here the detection method of Ref. [24], which combines matter wave interference with the technique of Bragg scattering [25]. Finally, we conclude in Sec. V.

II. PHASE IMPRINTING

Let us first remind the reader of the basic idea of the phase imprinting method, as presented in Ref. [24]. This

method consists of (i) passing a far-off resonant laser pulse through an absorption plate whose absorption coefficient depends on the rotation angle φ around the propagation axis, and (ii) creating the corresponding Stark shift potential inside a BEC by imaging the laser pulse onto the condensate. This leads to a φ-dependent shift of the phase of the condensate wave function. This method is very efficient and robust, and allows for the engineering of a variety of excited states of BEC containing vortices. In the ideal case the method allows us to generate genuine vortices with integer angular momenta. In the presence of imperfections, typically more complex vortex patterns are generated.

Before we turn to details, we should stress that the dynamical generation of vortices differs from the case of rotating traps, in which a *pure vortex* state with angular momentum $L_z=1$ (in units of $\hbar$) is selected in the process of reaching the thermal equilibrium. In our case, the generation of *pure* vortices requires tuning of parameters which is hard, but not impossible, to achieve in experiments. Our method is suitable for the creation of generic states with *vorticity* [26]. The scenario of vortex creation is such that the state without any topological defects during or right after the phase imprinting is dynamically unstable and develops typically into a state with several vortex lines, around which the circulation of velocity does not vanish. Some of these vortices are pushed away from the center of the trap to the regions of low density where they remain hardly observable. In effect, an ''ideal'' single vortex or vortex arrays can be created in the middle of the trap. These structures seem to be dynamically stable and their lifetime definitely is sufficiently long to allow for experimentally feasible detection. It is one of the main goals of this section to illustrate this scenario of topological defect creation (somewhat similar to Carman instability in nonlinear optics [27]) with numerical simulations.

The dynamics of BEC, and thus the process of creation and evolution of vorticity at zero temperature, is well described by the time-dependent Gross-Pitaevskii equation for the wave function $\psi(\mathbf{r},t)$,

$$i\hbar\partial_t\psi=\left(\frac{-\hbar^2\nabla^2}{2M}+V_{NL}(\mathbf{r},t)+V_t(\mathbf{r})+V_l(\mathbf{r},t)\right)\psi, \quad (1)$$

where $V_t(\mathbf{r})=M(\omega_x^2x^2+\omega_y^2y^2+\omega_z^2z^2)/2$ is the external trap potential that we assume to be harmonic, M is the mass of the atom, and $\omega_x,\omega_y,\omega_z$ are the trap frequencies. The nonlinear term $V_{NL}(\mathbf{r},t)=g|\psi(\mathbf{r},t)|^2$ describes the mean-field two-body repulsive interaction whose strength g is related to the scattering length a by $g=4\pi N\hbar^2a/M$, where N is the total number of condensed particles. The term $V_l(\mathbf{r},t)$ describes an effective potential created by an external laser beam impinging on the condensate after passing through a plate with an appropriately modulated absorption coefficient. In the following we will study the two-dimensional version of Eq. (1), in which we replace g by g/D, where D is the characteristic depth chosen such that the ground-state chemical potentials of the three-dimensional (3D) and two-dimensional (2D) systems are equal. We have checked that our 2D calculations agree perfectly with the real 3D ones in the case of disk-shape geometry. We also expect that in the case of other geometries our method of generating vortices will be equally efficient. However, the further evolution of vortices might lead to different instabilities [28].

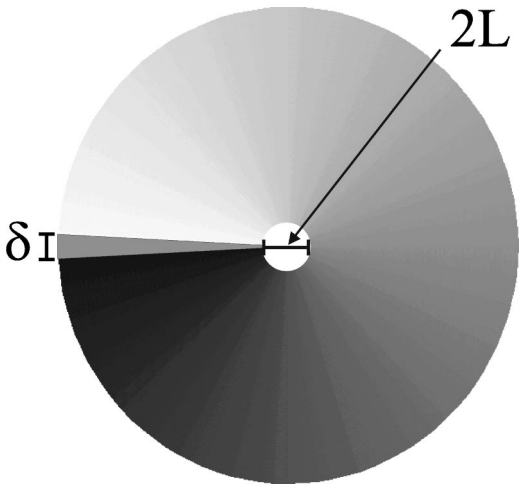

FIG. 1. Absorption plate. L is the radial extension on which the absorption profile was smoothed in our simulations, whereas δ is the angular extension of the smoothing.

We consider a short pulse of light with a typical duration of the order of fractions of microseconds with a properly modulated intensity profile. If the incident light is detuned far from the atomic transition frequency its main effect on the atoms is to induce a Stark shift of the internal energy levels. As the intensity of light depends on the position, the Stark shift will also be position dependent as will be the phase of the condensate. As a result, the laser pulse creates vorticity in a Bose-Einstein condensate initially in its ground state.

The topological defect introduced by a vortex is related to the behavior of the phase of the wave function at the vortex line: the phase ''winds up'' around this line, i.e., it changes by an integer multiple m of 2π on a path surrounding the vortex. Index m is the vortex charge. The light beam, before impinging on the atomic system, is shaped by an absorption plate whose absorption coefficients varies linearly with the rotation angle φ around the plate axis (see Fig. 1). As a result, $V_l(\mathbf{r},t)$ depends on cylindrical coordinates, on the distance from the propagation axis ρ, and the azimuthal angle φ.

In the ideal case this absorption plate causes a real jump of the potential at, say $\varphi=0$. In this case we can model the potential for $0\leqslant t\leqslant T$ by

$$V_l(\rho,\varphi)=\begin{cases}\hbar I\varphi\sin^2(\pi\rho/2L) & \text{for } \rho\leqslant L,\\ \hbar I\varphi & \text{for } \rho>L,\end{cases} \quad (2)$$

being zero for other times. Here T is the (square) pulse duration, whereas I denotes the characteristic Stark shift (proportional to the laser intensity); L is the characteristic length scale, on which the absorption profile is smoothed in our calculations in the vicinity of the propagation-rotation axis. As has been discussed in Ref. [24] the use of more realistic temporal pulse shapes does not change the results signifi-

cantly. In the following we will use square pulses, since it allows us to control the pulse area in a simpler manner.

The characteristic time and length scales for the BEC that we consider are milliseconds and micrometers, respectively [29]. Note that for this parameter range T is short ($\simeq \mu$s) and $\hbar I$ is much larger than other energy scales. Thus, the dynamical effect of $V_l(\rho,\varphi)$ corresponds approximately to a phase imprinting. Since during the interaction with the laser, all other terms in Eq. (1) can be neglected, the wave function after switching off the pulse becomes

$$\psi(\mathbf{r},T)=\exp[-iTV_l(\rho,\varphi)/\hbar]\psi(\mathbf{r},0). \tag{3}$$

For the ideal case, choosing $IT=m$, we get the desired phase dependence characteristic for a pure vortex state. Unfortunately, the above picture is oversimplified because the wave function (3) does not necessarily vanish at the vortex line ($\rho=0$), which signifies infinite kinetic energy and its nonphysical character. A correct and precise description requires that one has to solve the full dynamics of the system for $0 \leqslant t \leqslant T$, taking especially into account the kinetic energy term. Moreover, realistic absorption plates cannot generate the singularity in the φ dependence of V_l. For this reason we smooth the φ dependence of the intensity I on the scale of δ radians (see Fig. 1). Phase imprinting with this smoothed intensity distribution cannot generate pure vortex states—it can, however, as we shall see below, generate in a controlled way states with predetermined vorticity.

In this paper we have used essentially the same numerical method as in Ref. [24]. The Gross-Pitaevskii equation was solved using the split operator method in 2D (the x and y planes). The simulations were divided into two stages: the initial excitation stage of duration $T\simeq 0.16$ μs, with about 1000 time steps, and the second stage with a characteristic time scale of milliseconds, and about 1000 steps/ms. We have assumed that initially a condensate containing $N=100\,000$ rubidium atoms (with $a=5.8$ nm) was trapped in a disk-shaped trap of frequencies $\omega_x=\omega_y=2\pi\times 30$ Hz, $\omega_z=2\pi\times 300$ Hz. In this case the condensate radius was about 15 μm. We have used $I=6\times 10^6$ Hz, and adjusted T to obtain the desired values of the pulse area ($IT\simeq 1,2,\ldots$). The ρ dependence of the potential V_l was smoothed with $L\simeq 1.7$ μm, and the φ dependence with $\delta\simeq 0.04-0.15$ rad. The smallest possible value of $\delta\simeq 0.04$ rad was determined by the spatial grid size which typically was 512×512 points in a 40×40 μm^2 box. During the dynamics, after switching off the laser, the following quantities are conserved: the wave-function norm, the mean energy, and the mean z component of the angular momentum. They were monitored in order to control the accuracy of the numerics. The first two quantities were constant within the accuracy of the method, the third one in some cases exhibited slow variations of the order of a percent.

The summary of the results of [24] is as follows: the ''ideal absorption'' plate (with $\delta=0.04$) allows for perfect single vortex generation. This is not much influenced by focusing the laser slightly off center, or by using $\delta=0.15$. Of course, graduate degradation of the vortex pattern is expected as both of this imperfections increase.

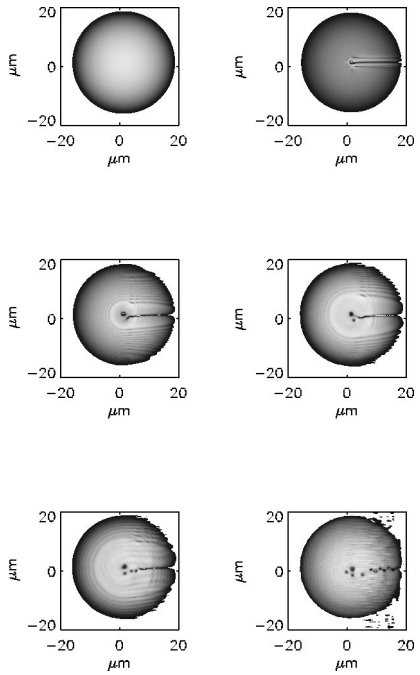

FIG. 2. BEC density during and right after the phase imprinting for the case of an ideal absorption plate with $\delta=0.04$ rad, and a sharp jump in the optical potential on the scale of the grid. The time of impinging was equal to $2.5/I$. One observes the characteristic valley in the density along the phase jump. The valley decays into vortices. The movie presents snapshots taken at times varying from $t=0$ up to $t=1.6$ ms.

A. Vortex formation

One of the major fundamental questions is how the nonzero circulation, i.e., a topological defect is introduced into the system during the phase imprinting. The scenario of vortex creation can be at best illustrated in conditions in which the pulse area is not integer. This is shown in Fig. 2 where we present a ''movie'' showing the condensate density during the imprinting of a phase $2.5(2\pi)$, and at later times until 1 ms.

Here, the case of an ideal absorption plate with $\delta=0.04$ rad, and a sharp jump in the optical potential on the scale of the grid is considered. During the imprinting or a little later, i.e., for the times of the order of microseconds a characteristic valley develops in the density profile along the phase jump line. The density adjusts here to the imprinted phase. The valley is, however, dynamically unstable, and within a time scale of fractions of milliseconds breaks down into a certain number of vortices. The vortices created in the middle of the trap seem to be dynamically stable. In Fig. 2 these are two vortices represented by the thick black dot in the middle of the trap (the resolution of the figure does not allow us to see the vortices separation). This vortex pair is surrounded by several single vortices that flow away along spiral trajectories toward the outer regions of the condensate.

The valley in the density profile reaches within a fraction of milliseconds a size corresponding to the condensate healing length. The time scale of the density adjustment corresponds to the inverse of the characteristic frequency, determined by the mean-field energy in the condensate $g/\hbar V$,

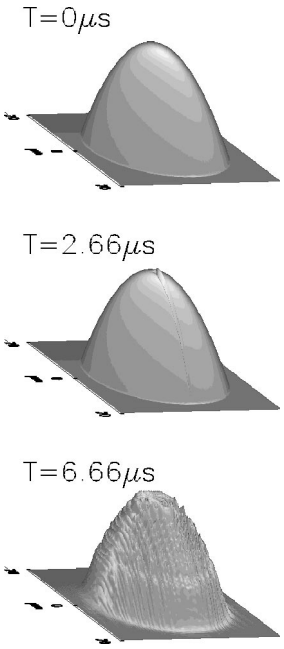

FIG. 3. BEC density during and right after the phase imprinting for the case of an ideal absorption plate with $\delta=0.04$ rad, and a sharp jump in the optical potential on the scale of the grid. The time of impinging was equal $2\pi/I$. One observes that the characteristic valley in density along the phase jump is very narrow, but visible. The valley decays into vortices. The movie presents snapshots taken at times $t=0$, $t=2.66$ μs, and $t=6.66$ μs.

where V is the volume of the condensate ($V\simeq 15\pi\times 15\times 4$ μm^3). It is the time required by the second sound to travel over a distance of the order of the healing length.

The scenario of introducing the topological defects into the system is similar to the Carman instability in nonlinear optics [27]. Dynamical instabilities play an essential role here. Basically, the mechanism of vortex creation is the same in the case of laser pulses with the area being an integer multiple of 2π. In this case, however, the width of the valley is much smaller, i.e., the valley is much steeper. It follows from our simulation that dynamical instability in such a situation appears much faster, and therefore the time scale for vortex formation is much shorter. This is illustrated in Fig. 3.

B. Multivortex formation

By adjusting the area of the pulse it is possible (using a single absorption plate) to create multivortex arrays, similarly as in the experiments of ENS [4]. We have performed a detailed analysis of the final vortex configuration in the function of the pulse area. We present these results obtained for a Rb condensate and the same trap parameters as above in Table I. As expected, increasing the area leads to the formation of regular arrays of more and more vortices. Such configurations (which are stationary in rotating traps [13]) undergo slow rotation in the nonrotating trap, but seem to be nevertheless dynamically stable over the time scales of at least 100 ms, but most probably much longer.

Generally, speaking the table shows that when the pulse area is close to $2\pi k$, with $k=1,2,\ldots$, then the corresponding k vortex array in the center of the trap is formed. For areas between the integer values it may happen that we have also some number of vortices, but this number is not a monotonic function of the pulse area.

III. PHASE IMPRINTING WITH MULTIPLE PLATES

The results above show that phase imprinting allows for controlled vortex generation. This fascinating possibility of macroscopic quantum state engineering can be realized with a high precision if the multiple absorption plates are used. In order to understand better the possibilities of coherent con-

TABLE I. Number of vortices created with the phase imprinting method as a function of the laser pulse area (in units of 2π).

Area (2π)	Description
0–0.133	No vortex
0.133–0.5	From 1 up to 8 vortices near the border of the condensate
0.5–0.8	1 vortex in the center of the trap and from 1 to 8 vortices near the border of the condensate
0.8–1.2	1 vortex in the trap center
1.2–1.4	1 vortex in the trap center and several vortices near the border of condensates
1.4–1.533	No vortex in the trap center but about 4 vortices near the trap center and 2–3 near the border of the condensate
1.533–1.733	2 vortices in the trap center and 1–2 vortices near the border
1.733–2.2	2 vortices in the trap center
2.2–2.2466	2 vortices in the trap center and from 3 up to 8 vortices near the border
2.466–3.666	3 vortices in the trap center and 2 near the border of the condensate
3.666–4.2	4 vortices in the trap center
4.2–4.466	4 vortices in the trap center and 3–5 vortices out of trap center
4.466–5.2	5 vortices in the trap center
5.2–5.533	5 vortices in the trap center and from 1 to 5 near the border of the condensate
5.33–6.2	6 vortices in the trap center

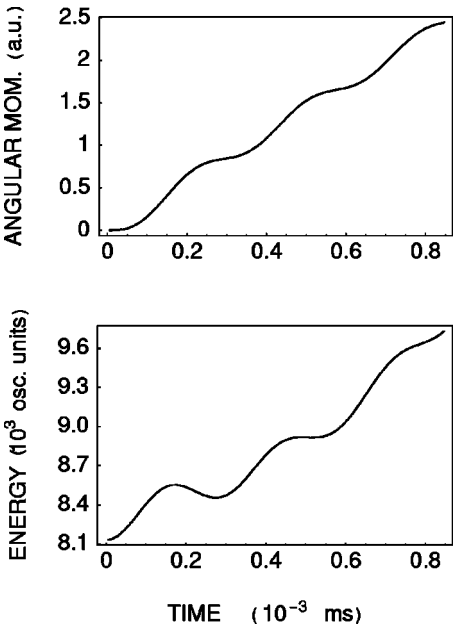

FIG. 4. Angular momentum per atom and the energy of the condensate in the first 0.84 μs when the laser pulse acts on the condensate through the single absorption plate. The number of atoms $N=50\,000$ and the trap frequency $\omega=2\pi\times30$ Hz.

trol in the system considered, we will first discuss the vortex arrays generation as a function of the absorption plate parameters in more detail.

A. Vortex arrays with a single absorption plate

To investigate the generation of multiple charged vortices we have first solved the Gross-Pitaevskii equation with the effective potential created by an external laser beam passing through a single absorption plate. Choosing $IT=3$ (here $T\approx0.84$ μs) we get the desired phase for the $m=3$ vortex state. In Fig. 4 we plot the angular momentum acquired by the condensate being initially in the ground state as well as the energy of the condensate during the process of phase imprinting. The local minima that appear in the curve describing the condensate energy correspond to the imprinting of the phase for the $m=1$ vortex state (pulse duration of 0.28 μs) and for the $m=2$ vortex state (pulse duration of 0.56 μs).

It turns out that the extent of the region on which the absorption profile is smoothed plays an important role. It affects the position of the created vortex. For a small diameter of smoothing area the vortex is generated near the center of the trap and rapidly decays into a few (for $m>1$) not ''well developed'' vortices. These vortices form regular geometrical patterns only when their distance to the trap center is very small. Therefore, they are also close to each other and it is very difficult to distinguish them. The descendant vortices become well separated only when the size of the smoothing region gets large enough. It is demonstrated in Fig. 5 where the radius of the region smoothing the absorption profile equals 4.0 oscillatory lengths (the oscillatory length ≈2.0 μm). However, in such a case the vortices are always

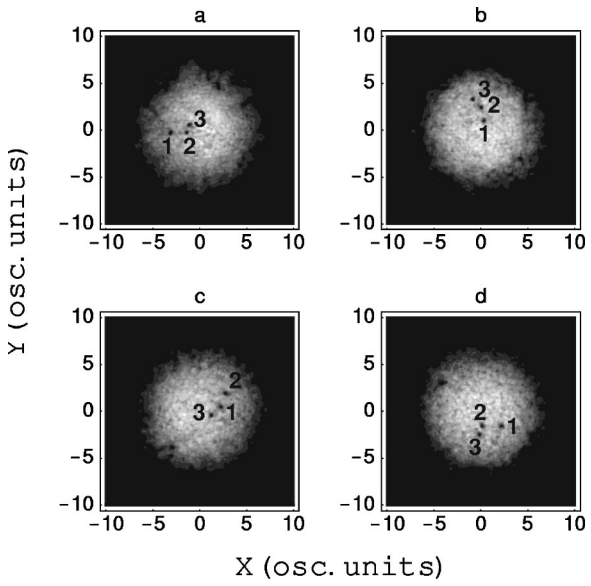

FIG. 5. Snapshots of the condensate density after illuminating through the single absorption plate (under the same conditions as for Fig. 4). The successive frames describe the moments: (a) 10.6 ms, (b) 15.9 ms, (c) 21.2 ms, and (d) 26.5 ms. The vortices (black dots) are marked by the numbers.

shifted away from the center of the trap and do not form regular geometrical patterns. Because of this fact the phase imprinting method with the single absorption plate does not allow for the efficient creation of multiple symmetric vortex configurations.

The vortices (black dots marked by the numbers) circulate both the trap center as a whole and individually the geometrical center of the vortex configuration. Closer inspection shows (Fig. 6) that the geometrical center rotates the center of the trap at an approximately constant radius, whereas the relative motion is a sum of oscillatory motion and rotation.

B. Vortex arrays with multiple absorption plates

To generate symmetric vortex configurations we propose the following extension of the phase imprinting method. In-

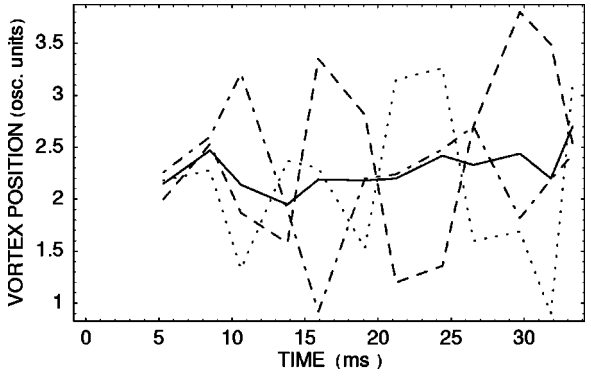

FIG. 6. Relative (with respect to the geometrical center) position of the vortex as a function of time. Parameters are the same as in Fig. 5; particular lines correspond to vortex No. 1 (dashed-dotted line), vortex No. 2 (dotted line), and vortex No. 3 (dashed line). The solid line follows the distance of the geometrical center of the vortex configuration from the center of the trap.

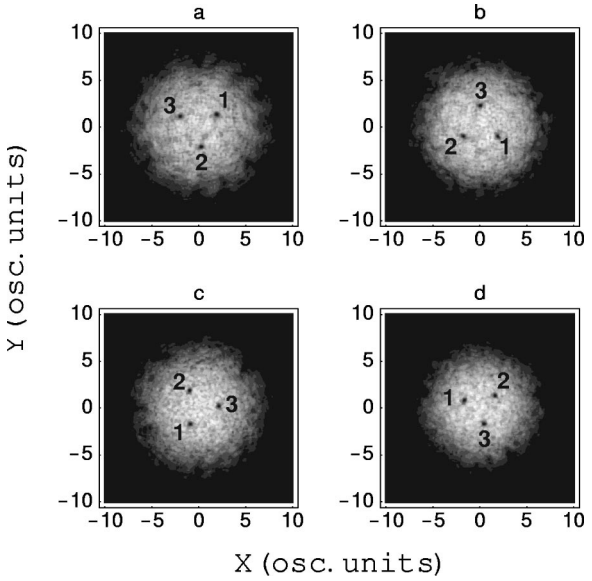

FIG. 7. Evolution of the symmetric three-vortex configuration. The array of vortices circulates as a whole around the center of the trap. The frequency of this rotation is higher than the frequency of the trap and depends on the size of the configuration, i.e., the distance of the vortices from the center of the trap (see Fig. 8). The consecutive snapshots correspond to instants at (a) 9.5 ms, (b) 12.7 ms, (c) 17.0 ms, and (d) 21.2 ms after the imprinting of the phase. The absorption profile for every plate is smoothed over the region of the radius of 4.0 oscillatory lengths, and the jumps of the potential caused by the plates are located every 120°.

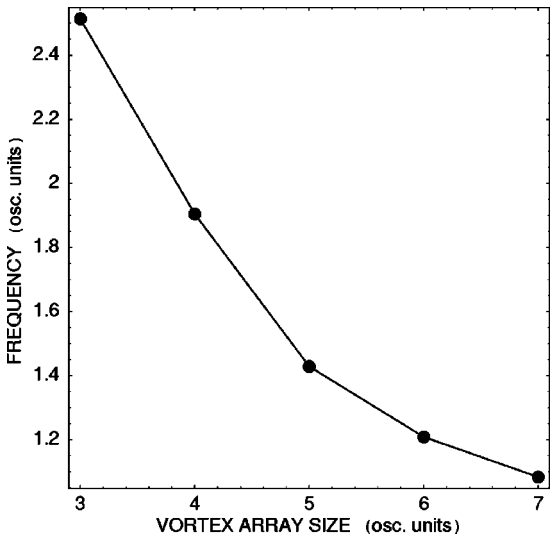

FIG. 8. Frequency of the rotation of the three-vortex array as a function of its size.

stead of a single absorption plate we use several of them arranged one by one. The parameters of the laser pulse impinging on the condensate are taken in such a way that passing the pulse independently through any plate the phase characteristic for a pure single vortex state is imprinted just as it was done before. However, now the direction of the jump of the potential caused by each plate is arbitrary as well as the size of the area where the absorption profile is smoothed. The overall action of a chain of the absorption plates is roughly a sum of individual results. This method allows for engineering arbitrary configurations of vortices, including also those with positive and negative vortex charge. Figure 7 illustrates the case of the symmetric 3-vortex (all positive) configuration. We find that once generated this configuration appears to be quite robust, except for the circulation around the center of the trap.

Changing the diameter of the space over which the absorption profile is smoothed we are able to generate the vortex configurations of different size. It turns out that the frequency of the circulation of the vortex array depends on that size; the smaller radius of the configuration implies higher frequency. The overall behavior is visible in Fig. 8. The frequency of the circulation is always higher than the frequency of the trap and the question can be raised about the link of the vortices created in such a way and the vortices that appear in the rotating trap.

Since the frequency of a rotation of the vortex around the center of the trap depends on the distance between the vortex and the center, by playing with this distance we can investigate the collisions between positive charged vortices. An example is presented in Fig. 9. An array of three vortices was generated with the help of three absorption plates with slightly different radii of smoothing area (4.0, 3.5, and 3.0 oscillatory lengths, respectively). Frame 9(b) shows the instant when vortex 1 maximally approaches vortex 2 and partially passes its velocity to vortex 2. Then vortex 2 accelerates and after some time collides with vortex 3 [frame 9(c)]. After the next 6 ms vortex 3 hits vortex 1 and then the above scenario is repeated.

The dynamics of the vortex motion gets more complex when the number of vortices increases. Figure 10 shows a qualitatively new behavior. It turns out that in such a complex system vortices ''like'' to group in pairs. Once the pair of vortices is created, it rotates around its geometrical center

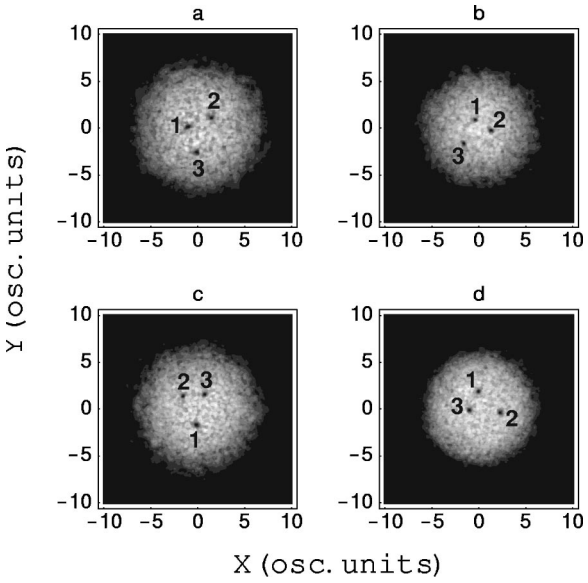

FIG. 9. Nonsymmetric three-vortex configuration at different times: (a) 14.8 ms, (b) 16.4 ms, (c) 23.3 ms, and (d) 29.7 ms.

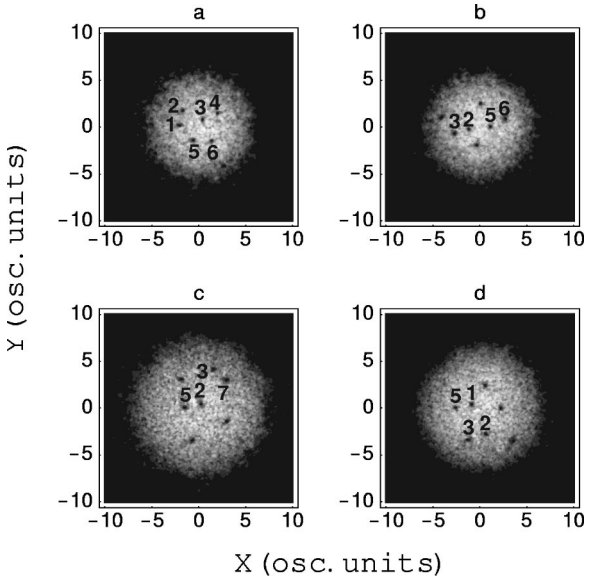

FIG. 10. Illustration of ''pairing,'' a phenomenon that appears in multivortex configurations. Frames (a), (b), (c), and (d) correspond to evolutionary times 24.4, 42.9, 47.1, and 68.8 ms, respectively.

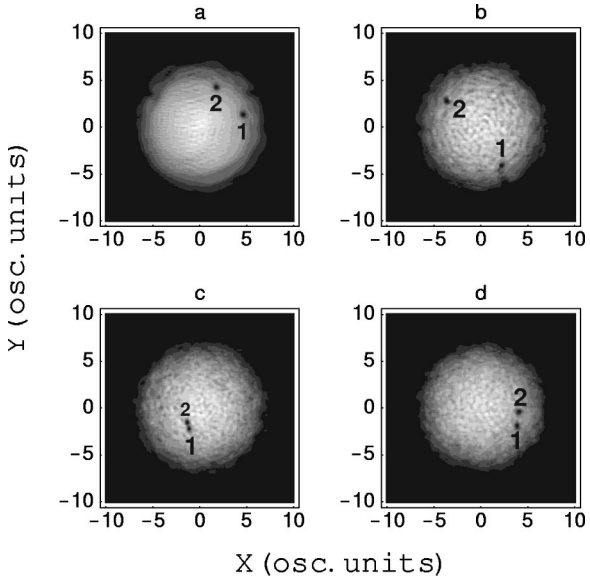

FIG. 11. Example of dynamics of the vortex configuration including both positive and negative charged vortices. The snapshots are taken at times of (a) 4.2 ms, (b) 11.7 ms, (c) 20.2 ms, and (d) 23.3 ms. No annihilation of vortices occurs during the collision [frame (c)].

as well as the center of the trap. This motion continues until the collision with the other pair or a single vortex happens. Then the pair is broken and likely the exchange of vortices occurs; a new pair of vortices is built. In the case of Fig. 10 the condensate was prepared with the help of six absorption plates. Frames 10(a)–10(d) are examples of vortex pairs appearing in the condensate. From these frames it is also clear that there is a mechanism for vortex exchange.

Finally, we have investigated the simplest vortex configurations with positive and negative charged vortices. The phase imprinting method with multiple absorption plates seems to be an ideal tool for generating such configurations. The simplest case is a one positive charged vortex and one negative charged vortex. For that we need two plates with the absorption coefficient modulated clockwise for one plate and counterclockwise for another one. The radius of the region over which the absorption profile is smoothed is slightly different for both plates (3.5 and 2.0 oscillatory units) and the jump of the potential is taken along $\phi=0$. The numerical analysis shows that almost no angular momentum is transferred to the condensate in this case. Instead of that, a pair of opposite charged vortices with large momentum is created; see Fig. 11. The vortices repel each other as well as the ''edge'' of the condensate [frames 11(a) and 11(b)], collide after 20.2 ms [frame 11(c)], and then move together through the condensate over a few ms without an annihilation [frame 11(d)].

IV. DETECTION OF VORTEX ARRAYS USING INTERFERENCE

Multiple vortices and vortex arrays can be detected using the same method of self-interference that we proposed in Ref. [24]. This method is analogous to the ones used in nonlinear optics [30]. In the context of matter waves similar methods were proposed in Refs. [26,31]. Our idea is to combine this method with the recently developed techniques of Bragg diffraction for BEC manipulation [25].

Efficient detection is one of the most important aspect of the investigation of vortices. Experimentally monitoring density profiles with the necessary resolution is difficult, since the vortex core is very small. This can be circumstanced by opening the trap (see for instance [4,6]). Although stable minima arranged in regular patterns in the density profile are very strong indications for the existence of vortices arrays, but the very important issue is to monitor how a phase of the wave function changes close to these minima. In fact, vortices are topological defects of the phase of the wave function. The phase can be detected only in an interference measurement. Such interference measurements are routinely done in nonlinear optics [30]. In the context of BEC, they were first proposed by Bolda and Walls [26], who considered the interference of two condensates moving toward each other. If both condensates are in the ground state (no vortices), one expects interference fringes as those observed by Ketterle *et al.* [32]. In the case of interference of one condensate in the ground state with the second one in the $m=1$ vortex state, a forklike dislocation in the interference pattern appears. The distance between the interference fringes is determined by the relative velocity of the condensates, which can be controlled experimentally. This is a very efficient and clear method of vorticity detection (see Fig. 12). It requires, however, the use of two independent condensates.

In Ref. [24] we have proposed to combine the interference method with the recently developed Bragg diffraction technique [25], which has been for instance successfully used in a four-wave-mixing experiment [33]. The idea is to transfer part of the atoms coherently to another momentum state using one or several stimulated two-photon Raman scattering processes. The procedure is as follows.

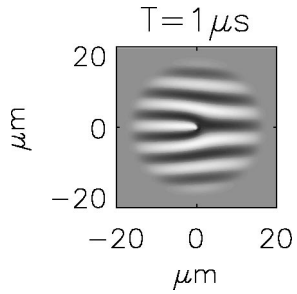

FIG. 12. Interference pattern of a singe vortex with the plane wave running in the direction from the bottom to the top. One can easily see a forklike structure in the middle of the interference pattern; this provides the proof of winding of the phase around the center of the condensate. The vortex has been created using a very small step in the intensity profile $\delta \simeq 0.04$ rad.

(i) First we create the vortex, or vorticity state in the trap.

(ii) We open the trap and let the condensate expand.

(iii) When the density is reduced to values for which nonlinear interactions are negligible, we apply the Bragg pulses. Part of the wave function attains a phase factor that signifies the fact that the corresponding momentum was transferred to part of the atomic sample.

If the resonant width of the Raman transition is narrower than the wave function spreading in the momentum space (in our case the velocity spread is typically about 0.12 μm/ms) not all momentum components can experience the shift. In that case the contrast of interference fringes will be reduced. One can, however, correct for this by adiabatic opening the trap before applying Bragg pulses. The resulting wave function is the superposition of two vortex (or vorticity) states moving apart from each other, with a velocity that can be easily controlled by the choice of the angle between the Bragg beams. In the following we will use velocities of the order of 1 mm/s, which allow for efficient detection after 4–5 ms when the vortices are about 5 μm apart.

(iv) Detection consists of optical imaging that is accomplished within a few microseconds. The interference patterns (see Fig. 13) have a characteristic length scale of a few micrometers.

Below we present the results of numerical simulation of this detection scheme. The corresponding interference patterns were obtained for the case $\delta \simeq 0.04$ rad, for 3- and 6-vortex arrays. The interference patterns show multifork dislocation, termed by us ''quantum peacocks,'' which are presented in Figs. 14 and 15. The shape of the interference pattern here allows us to unambiguously detect the vortex number and the array configuration, and to provide information about the phase of the wave function.

The interference method is also very useful in understanding the scenario of topological defect creation in the condensate. We illustrate this point in the movie in Fig. 16. The presented interference pattern can hardly be measured experimentally (because of the short time scale of the process), but we present them in order to get more insight and understanding of the process of generation of an ideal single vortex presented in Fig. 3. The sharp jump in the optical potential has very large gradients and introduces a very strong

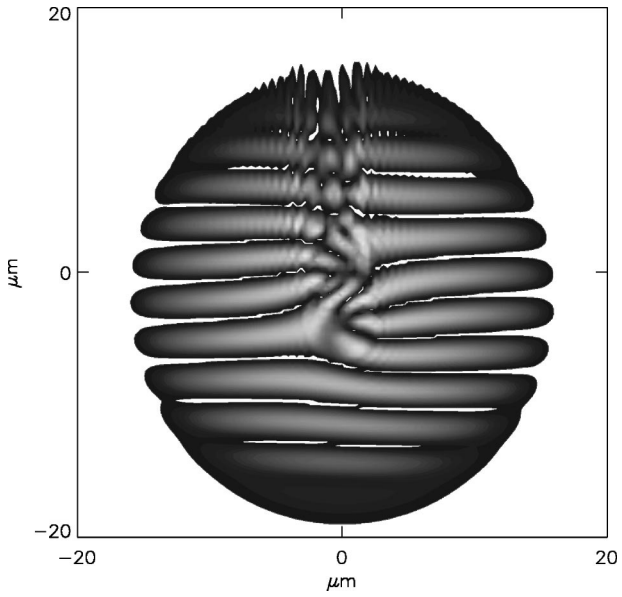

FIG. 13. Interference pattern of a three-vortex array, 1 ms after applying Bragg pulses transferring momentum to a part of the condensate (along the *y* axis in the plane of the figure), which coherently pushes a half of the condensate with velocity 0.01 mm/s. The incident pulse was focused at the trap center, had a sharp step in the intensity profile ($\delta = 0.04$), and had the area of 2π.

force, pushing the atoms transversely away from the region of the potential jump. The density valley is created already after 1.33 μs, but the topological defect is not present (interference fringes are deformed but not broken). In successive snapshots we see how dynamical instabilities lead to such a large shift and deformation of the fringes that finally brake and join smoothly with the corresponding nearest upper

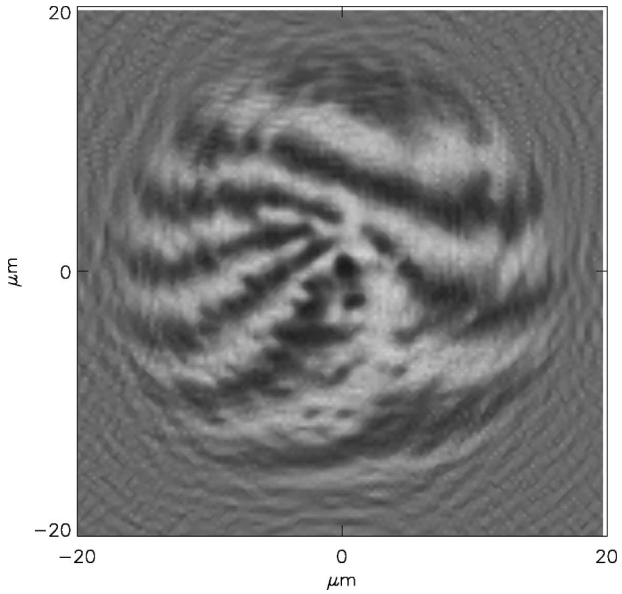

FIG. 14. Interference pattern of a three-vortex array with the plane wave of Fig. 12. The vortex array has been created by applying a laser pulse modulated by the absorption plate with $\delta = 0.04$ rad. The time of impinging was equal to $6\pi/I$.

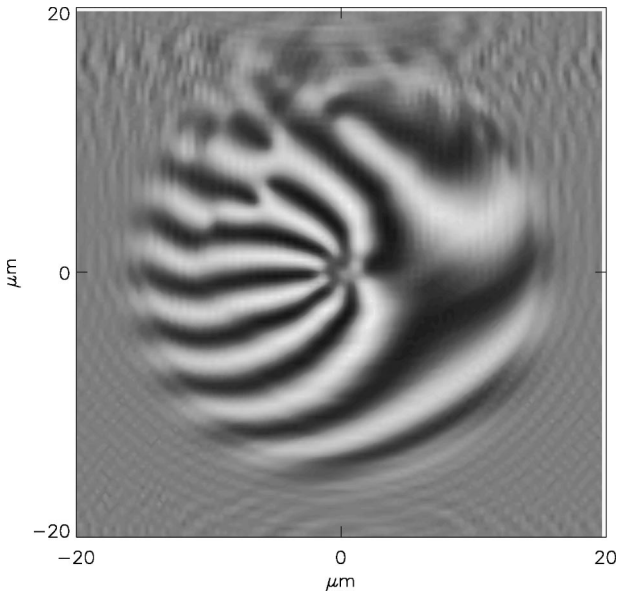

FIG. 15. Interference pattern of a six-vortex array with the plane wave. The array has been created by applying a laser pulse modulated by the absorption plate with $\delta = 0.04$ rad. The time of impinging was equal to $12\pi/I$.

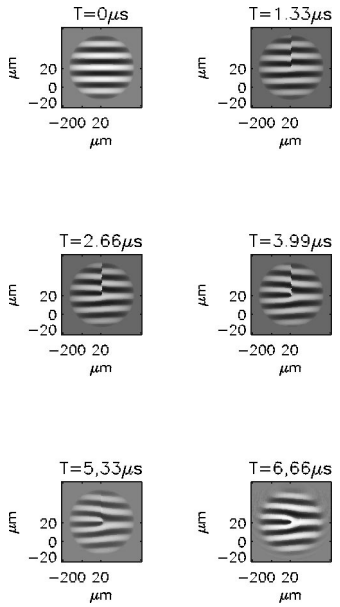

FIG. 16. The movie illustrating generation of the single vortex presented in Fig. 3 by using the interference patterns.

neighbor. This occurs for all, except the central fringe that builds a very clear fork pattern after 6.66 μs, corresponding to the topological defect.

V. CONCLUSIONS

In this paper we have studied theoretically the generation of vortices by phase imprinting in trapped Bose-Einstein condensates. Phase imprinting is achieved by passing a short off-resonance laser pulse through an appropriately designed absorption plate, and impinging it on a condensate. Apart from answering the fundamental question how the circulation and the vortex are introduced into the system, we have concentrated on the practical questions of controlling the generation of vortices and vortex arrays, their dynamics, and their detection. Although so far the phase imprinting method in the version discussed in this paper has only been used to generate dark solitons in BEC, we hope that in the future some experimental groups will apply the phase imprinting method to study vortex generation, dynamics, and superfluidity in trapped BEC. The theory presented in the present paper should help to plan and design such experiments [34].

ACKNOWLEDGMENTS

M.G. acknowledges support by Polish KBN Grant No. 2 P03B 078 19. This work has been supported by Deutsche Vorschungsgemeinschaft (SFB 407, Graduiertenkolleg 282), and ESF PESC Programm No. BEC2000+. We thank G. Birkl, W. Ertmer, L. Pitaevski, L. Santos, K. Sengstock, K. Staliunas, and S. Stringari.

[1] C. Raman, M. Köhl, R. Onofrio, D. S. Durfee, C. E. Kuklewicz, Z. Hadzibabic, and W. Ketterle, Phys. Rev. Lett. **83**, 2502 (1999).
[2] R. Onofrio, C. Raman, J. M. Vogels, J. R. Abo-Shaeer, A. P. Chikkatur, and W. Ketterle, Phys. Rev. Lett. **85**, 2228 (2000).
[3] P. O. Fedichev, G. V. Shlyapnikov, and J. T. M. Walraven, Phys. Rev. Lett. **80**, 2269 (1998).
[4] K. W. Madison, F. Chevy, W. Wohlleben, and J. Dalibard, Phys. Rev. Lett. **84**, 806 (2000).
[5] F. Chevy, K. W. Madison, and J. Dalibard, Phys. Rev. Lett. **85**, 2223 (2000); recently also the MIT group observed multivortex arrays, see J. R. Abo-Shaeer, C. Raman, J. M. Vogels, and W. Ketterle (unpublished).
[6] M. R. Matthews, B. P. Anderson, P. C. Haljan, D. S. Hall, C. E. Wieman, and E. A. Cornell, Phys. Rev. Lett. **83**, 2498 (1999).
[7] O. M. Maragó, S. A. Hopkins, J. Arlt, E. Hodby, G. Hechenblaikner, and C. J. Foot, Phys. Rev. Lett. **84**, 2056 (2000).
[8] D. Guery-Odelin and S. Stringari, Phys. Rev. Lett. **83**, 4452 (1999).
[9] S. Burger, K. Bongs, S. Dettmer, W. Ertmer, K. Sengstock, A. Sanpera, G. V. Shlyapnikov, and M. Lewenstein, Phys. Rev. Lett. **83**, 5198 (1999).
[10] J. Denschlag, J. E. Simsarian, D. L. Feder, C. W. Clark, L. A. Collins, J. Cubizolles, L. Deng, E. W. Hagley, K. Helmerson, W. P. Reinhardt, S. L. Rolston, B. I. Schneider, and W. D. Phillips, Science **287**, 97 (2000).
[11] R. J. Marshall, G. H. C. New, K. Burnett, and S. Choi, Phys. Rev. A **59**, 2085 (1999); P. D. Drummond and J. F. Cornay, e-print cond-mat/9806315.
[12] F. Dalfovo and S. Stringari, Phys. Rev. A **53**, 2477 (1996).
[13] D. A. Butts and D. S. Rokhsar, Nature (London) **397**, 327 (1999).

[14] D. L. Feder, Ch. W. Clark, and B. I. Schneider, Phys. Rev. Lett. **82**, 4956 (1999).
[15] J. E. Williams and M. J. Holland, Nature (London) **401**, 568 (1999).
[16] P. O. Fedichev and G. V. Shlyapnikov, Phys. Rev. A **60**, R1779 (1999); A. A. Svidzinsky and A. L. Fetter, Phys. Rev. Lett. **84**, 5919 (2000).
[17] B. Jackson, J. F. McCann, and C. S. Adams, Phys. Rev. Lett. **80**, 3903 (1998).
[18] B. M. Caradoc-Davies, R. J. Ballagh, and K. Burnett, e-print cond-mat/9902092.
[19] K. P. Marzlin and W. Zhang, Phys. Rev. A **57**, 3801 (1998).
[20] R. Dum, J. I. Cirac, M. Lewenstein, and P. Zoller, Phys. Rev. Lett. **80**, 2972 (1998).
[21] K. P. Marzlin, W. Zhang, and E. M. Wright, Phys. Rev. Lett. **79**, 4728 (1997).
[22] K. Staliunas, Appl. Phys. B: Lasers Opt. **71**, 555 (2000).
[23] C. O. Weiss, M. Vaupel, K. Staliunas, G. Slekys, and V. B. Taranenko, Appl. Phys. B: Lasers Opt. **68**, 151 (1999).
[24] Ł. Dobrek, M. Gajda, M. Lewenstein, K. Sengstock, G. Birkl, and W. Ertmer, Phys. Rev. A **60**, R3381 (1999).
[25] M. Kozuma, L. Deng, E. W. Hagley, J. Wen, R. Lutwak, K. Helmerson, S. L. Rolston, and W. D. Phillips, Phys. Rev. Lett. **82**, 871 (1999).
[26] E. L. Bolda and D. F. Walls, Phys. Rev. Lett. **81**, 5477 (1998).
[27] Y. S. Kivshar and B. Luther-Davies, Phys. Rep. **298**, 81 (1998).
[28] A. L. Fetter and A. A. Svidzinsky, J. Phys.: Condens. Matter **13**, R135 (2001).
[29] K. Bongs, S. Burger, G. Birkl, K. Sengstock, W. Ertmer, K. Rzążewski, A. Sanpera, and M. Lewenstein, Phys. Rev. Lett. **83**, 3577 (1999).
[30] I. V. Basistiy *et al.*, Opt. Commun. **103**, 422 (1993); L. V. Kreminskaya, M. S. Soskin, and A. I. Khizhnyak, *ibid.* **145**, 377 (1998); J. F. Nye and M. V. Berry, Proc. R. Soc. London, Ser. A **336**, 165 (1974).
[31] F. Dalfovo, S. Giorgini, and L. P. Pitaevskii, Rev. Mod. Phys. **71**, 463 (1999).
[32] M. R. Andrews, C. G. Townsend, H. J. Miesner, D. S. Durfee, D. M. Kurn, and W. Ketterle, Science **275**, 637 (1997).
[33] L. Deng, E. W. Hagley, J. Wen, M. Trippenbach, Y. Band, P. S. Julienne, J. E. Simsarian, K. Helmerson, S. L. Rolston, and W. D. Phillips, Nature (London) **398**, 218 (1999).
[34] To our knowledge the presented method provides a rather rare opportunity of controlled generation of vortex-antivortex pairs; for an alternative see J.-P. Martikainen, K.-A. Suominen, L. Santos, T. Schulte, and A. Sanper, Phys. Rev. A (to be published).